## Title

Radular stylus of Cryptochiton stelleri: A multifunctional lightweight and flexible fiber-reinforced composite



## Authors

Pohl, Anna
Herrera, Steven A
Restrepo, David
et al.

## Publication Date

2020-11-01

## DOI

10.1016/j.jmbbm.2020.103991

journal of the mechanical behavior of biomedical materials 111 (2020) 103991

Contents lists available at ScienceDirect

Journal of the Mechanical Behavior of Biomedical Materials

journal homepage: http://www.elsevier.com/locate/jmbbm

# Radular stylus of *Cryptochiton stelleri*: A multifunctional lightweight and flexible fiber-reinforced composite

Anna Pohl [a,b,1], Steven A. Herrera [a,1], David Restrepo [c,d], Ryo Negishi [e,f], Jae-Young Jung [g,h], Chris Salinas [a], Richard Wuhrer [i], Tomoko Yoshino [e,f], Joanna McKittrick [g], Atsushi Arakaki [e,f], Michiko Nemoto [j], Pablo Zavattieri [c], David Kisailus [a,b,k,*]

[a] Materials Science and Engineering Program, University of California, Riverside, USA
[b] Department of Chemical and Environmental Engineering, University of California, Riverside, USA
[c] Lyles School of Civil Engineering, Purdue University, West Lafayette, USA
[d] Department of Mechanical Engineering, The University of Texas at San Antonio, USA
[e] Division of Biotechnology and Life Science, Institute of Engineering, Tokyo University of Agriculture and Technology, Tokyo, Japan
[f] Institute of Global Innovation Research, Tokyo University of Agriculture and Technology, Tokyo, Japan
[g] Materials Science and Engineering Program, University of California, San Diego, USA
[h] Department of Orthopaedic Surgery, University of California, San Francisco, USA
[i] Advanced Materials Characterization Facility, Western Sydney University, Australia
[j] Graduate School of Environmental and Life Science, Okayama University, Okayama, Japan
[k] Department of Materials Science and Engineering, University of California, Irvine, USA

ARTICLE INFO

*Keywords:*
Mollusk
Biocomposite
Force transduction
Flexible

ABSTRACT

Chitons are herbivorous invertebrates that use rows of ultrahard magnetite-based teeth connected to a flexible belt (radula) to rasp away algal deposits growing on and within rocky outcrops along coastlines around the world. Each tooth is attached to the radula by an organic structure (stylus) that provides mechanical support during feeding. However, the underlying structures within the stylus, and their subsequent function within the chiton have yet to be investigated. Here, we investigate the macrostructural architecture, the regional material and elemental distribution and subsequent nano-mechanical properties of the stylus from the Northern Pacific dwelling *Cryptochiton stelleri*. Using a combination of μ-CT imaging, optical and electron microscopy, as well as elemental analysis, we reveal that the stylus is a highly contoured tube, mainly composed of alpha-chitin fibers, with a complex density distribution. Nanoindentation reveals regiospecific and graded mechanical properties that can be correlated with both the elemental composition and material distribution. Finite element modeling shows that the unique macroscale architecture, material distribution and elemental gradients have been optimized to preserve the structural stability of this flexible, yet robust functionally-graded fiber-reinforced composite tube, providing effective function during rasping. Understanding these complex fiber-based structures offers promising blueprints for lightweight, multifunctional and integrated materials.

## 1. Introduction

Multifunctional materials are in high demand for aerospace, automotive and biomedical industries. Such engineered structures often need to be lightweight, flexible, and tough, as well as have integrated features such as utility at high temperature or in aqueous environments, exhibit biocompatibility, or demonstrate self-healing. In many of these systems, hybrid structures that demonstrate multiple functions utilize materials with dissimilar properties. However, material failure often occurs at the interfaces between two dissimilar materials. Thus, finding an effective and reliable way to integrate dissimilar materials is a challenge (Thomopoulos et al., 2013).

Often, dissimilar material properties can be integrated by using composite materials. Fiber-reinforced composites and functionally graded materials are two common types of composites (Chung, 2010; Kar, 2016). Fiber-reinforced composites offer exceptional

* Corresponding author. Materials Science and Engineering Program, University of California, Riverside, USA.
*E-mail address:* david.k@uci.edu (D. Kisailus).
[1] Co-first authors.

https://doi.org/10.1016/j.jmbbm.2020.103991
Received 16 February 2020; Received in revised form 22 May 2020; Accepted 13 July 2020
Available online 26 July 2020

strength-to-weight ratios and an anisotropic structure, which can be used to increase stiffness in a preferred direction (Mallick, 2007). However, many fiber-reinforced composites are limited by the lack of control over microstructure, interfaces, and often undergo delamination (Caprino, 1984). Furthermore, integration of multiple materials into region-specific locations in composite materials still proves challenging. In functionally graded materials, two or more dissimilar materials are gradually merged and thereby incorporate different properties into one component (Pompe et al., 2003; Udupa et al., 2014). Graded composites have advantageous physical properties and are used for various applications requiring resistance to contact deformation (Chung and Das, 2008; Krumova, M, Klingshirn, C et al., 2001; Suresh, 2001), temperature-based deformation (Shao, 2005) and offer biological compatibility via coupling with ceramic or metallic implants (Pompe et al., 2003). While structurally and functionally advantageous, the manufacturing of composite materials is often complicated and requires numerous production steps.

Nature presents various effective examples of integration of different materials in hierarchically assembled, multifunctional architectures (Gorb, 2008). Thereby, failure mechanisms are circumvented and various functions are enabled. Furthermore, many biological materials are lightweight, biocompatible and often function in aqueous environments. These natural systems have evolved over hundreds of millions of years under ambient conditions and with a limited selection of materials. Many biological structures incorporate both fiber-reinforcement as well as structural and chemical gradients in order to reduce interfacial stresses that exist between materials with significantly different material properties (Naleway et al., 2015). In biomineralized structures, such as arthropod cuticles, mollusk shells, and bone (Grunenfelder et al., 2014a; Meyers et al., 2008, 2013; Weaver et al., 2012; Yaraghi et al., 2016), the inorganic, stiff and hard minerals (e.g., calcium carbonate and phosphate, silica, iron oxide) are deposited around, or on flexible fibrous organic materials such as cellulose, collagen, keratin or chitin. In fact, non-mineralized biological composites such as fibrocartilage in ligaments of human femurs exist (Moffat et al., 2008). These flexible structures must balance bending and buckling resistance without significantly adding mass (Meyers et al., 2013). This combination of different material properties and the hierarchical assembly of inorganic and organic components results in materials with outstanding properties (Huang et al., 2019).

A group of organisms that produces unique multifunctional composite materials are chitons, herbivorous mollusks that live in the coastal zones worldwide, where they graze on rocks with a tongue-like organ (radula) to feed on algae growing on and inside these rocks (Brooker and Shaw, 2012; Kirschvink and Lowenstam, 1979; Lowenstam and Weiner, 1989; Nemoto et al., 2012; Nesson and Lowenstam, 1996; Wang et al., 2013). Due to their stiff and ultrahard teeth (modulus of 90–125 GPa and hardness 9–12 GPa) (Grunenfelder et al., 2014b; Weaver et al., 2010), chitons rasp away parts of the rock to access food, thereby undercutting and forming the mushroom-like rock formations (Fig. 1A, inset). The radula of chitons contains three primary components that fulfill different functions: (i) ultrahard teeth that are capped with a magnetite layer, each of which are attached to (ii) a semi-flexible, yet stiff, stylus that provides force transduction to the teeth, and (iii) a long and flexible belt that provides a substrate upon which tens of rows of teeth are supported. Hence, the tooth-stylus-belt radular system of chitons is an exceptional example for the integration of dissimilar materials into a multifunctional structure.

Here, we investigate the macrostructural features and subsequent mechanics of the stylus from one such chiton, *Cryptochiton stelleri* (Fig. 1A). This species lives in the North Pacific Ocean and is one of the largest and well-characterized chiton species (Ricketts et al., 1985; Towe and Lowenstam, 1967; Wang et al., 2013; Weaver et al., 2010). The radula of *C. stelleri* consists of a ribbon-like membrane that supports about 80 rows of tricuspid teeth that advance from infancy at the posterior end to fully mineralized mature teeth at the anterior end (Fig. 1C). Similar radular structures have been observed in other chiton species (Brooker and Shaw, 2012; Macey and Brooker, 1996). The teeth are arranged in two rows of major lateral teeth positioned on either side of the flexible radula membrane (Fig. 1E) and are supported by adjacent marginal teeth.

The teeth, and thus styli, experience extensive repeated mechanical loading during rasping. Hence, the styli need to provide mechanical support and force transduction to the teeth in order for the chiton to feed. However, the morphological and microstructural features that afford this unique structure, both flexibility and stiffness, have yet to be reported. Previous results as well as scanning electron microscopy (Fig. S1) reveal that the stylus is composed of continuous alpha-chitin fiber sheets that propagate from the leading edge of the stylus through the junction zone into the tooth (Wang et al., 2013; Weaver et al., 2010). Investigation of a stylus from a different species of chiton suggested an additional role as an ion transport pathway during biomineralization (Shaw et al., 2009). Here, we reveal the structure-mechanical function relationships in the stylus using a combination of video analyses, X-ray micro-computed tomography (μ-CT), nanoindentation and energy-dispersive X-ray spectroscopy (EDS). The experimental findings were implemented in finite element (FE) simulations, which identified the stress distribution in the stylus due to different tooth tip loading

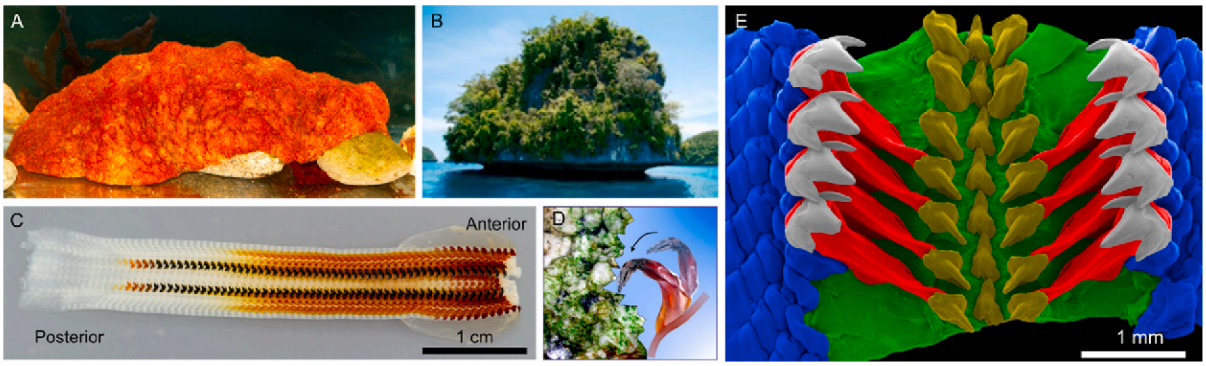


**Fig. 1.** The tooth-stylus-belt system of chitons is a prime example of a naturally occurring multifunctional composite that demonstrates coupling of dissimilar materials. A. Cryptochiton stelleri is an herbivorous marine mollusk found in the coastal zone of the North Pacific. B. Mushroom-shaped rock formed by the rasping action of chitons. C. The chiton radula consists of a ribbon-like membrane that houses about 80 rows of teeth at different stages of mineralization (the anterior end contains most mature teeth). D. Schematic drawing illustrating the rasping of a single tooth attached to the stylus on a rocky surface covered with algae. E. False colored SEM micrograph showing four rows of mature teeth (at the anterior end of the radula) used in grinding rock. Two rows of major teeth are positioned on either side of the flexible radula membrane. The major lateral teeth (grey) are attached on the proximal end by styli (red) to the radula membrane (green) and are adjacent to marginal teeth (yellow and blue). (For interpretation of the references to color in this figure legend, the reader is referred to the Web version of this article.)

directions during the rasping process. The outcomes of this study are promising for the design for next-generation lightweight, flexible composite materials useful for automotive (Araújo et al., 2017; Banea et al., 2018), aerospace (Khan et al., 2018; Scarselli et al., 2017), biotechnological or medical (Blanc et al., 2017) applications.

## 2. Materials and methods

### 2.1. Research specimen

*Cryptochiton stelleri* were obtained alive from Monterey Abalone Company (Monterey, USA). The rasping behavior of these chitons was observed by analyzing the videos taken while grazing on an acrylic tank of an artificial sea water system. The radulae were dissected from the chitons and subsequently serially dehydrated in EtOH (i.e., 10%, 30%, 50%, 70%, 80%, 90%, 100%, 100%, 100%, each for 10 min). The styli of *C. stelleri* were removed from the radula using tweezers and used for analysis by μ-CT, nanoindentation, EDS and electron microscopy.

### 2.2. μ-CT and 3D reconstruction

An intact tooth-stylus structure was scanned using X-ray micro-computed tomography (μ-CT) (Skyscan 1172, Bruker, USA). Serially dehydrated samples (as described in 2.1) were mounted to a 1 mm diameter steel pin using Loctite super glue liquid professional (Henkel, USA) and mounted on a chuck. For the scan, a rotation step size of 0.1125° and an exposure time of 10 s was used. The acceleration voltage was 80 kV and the isotropic voxel size was 1.4 μm. The images and three-dimensional reconstructed models were developed using Amira software (Thermo Fisher Scientific, USA). After reconstruction, cross-sectional dimensions were determined by creating triangular mesh models and saved into a 3D file extension format of the virtual reality modeling language (as known as VRL or VRLM).

### 2.3. Nanoindentation

Polished cross-sections of the stylus were prepared for nanoindentation by embedding the dehydrated styli in an epoxy resin (System, 2000 Laminating Epoxy Resin, Fiberglast, USA). The specimens were cut using a low-speed diamond saw (TechCut 4™, Allied High Tech Products, USA) and polished with progressively finer grades of silicon carbide paper and diamond lapping films.

Nanoindentation was performed on a longitudinal cross-section and six transverse cross-sections at defined positions along the long axis of the stylus. The samples were tested under ambient conditions in air using TI-950 nanomechanical testing system (Hysitron, USA) with a cube corner tip at a peak displacement of 250 nm. The grid size was adjusted to the size of the respective cross-section and the distance between the indents was 20 μm. The unloading curve of each indent was used to calculate the hardness and reduced modulus following the Oliver Pharr method (Pharr et al., 2009). The resulting modulus data were plotted using MATLAB.

### 2.4. EDS

Elemental mapping of polished cross-sections of the stylus were performed at 15 kV in a scanning electron microscope (Mira 3, Tescan, Czech Republic) equipped with a dual detector energy dispersive spectrometer (QUANTAX 400, Bruker Nano GmbH, USA).

### 2.5. Computational models

To create the computational models, the data from the CT-scans were segmented using Amira (Thermo Fisher Scientific, USA). Based on differences in density, separate stereolithography (STL) files were generated as well as an STL file of the whole tooth-stylus structure. The STL file for the entire tooth-stylus structure was imported into Geomagic Wrap (3D Systems, USA) for cleaning and generation of surfaces. Then, the cleaned part was exported into an. igs file and imported into Abaqus (Abaqus/Standard, Dassault Systèmes Simulia Corp, USA) for mesh generation. Finally, the mesh for the whole tooth-stylus structure was processed using and an in-house MATLAB file that correlates the mesh information with the STL files corresponding to each of the individual regions, allowing the selection of sets and assignment of material properties. This process simplified the material assignment operations rather than directly working the mesh file in Abaqus. The final model used for simulations consisted of 1,431,113 tetrahedral elements, and the behavior for each of the regions was assumed linear elastic. A schematic of the different material sets, and the mechanical properties used for each set are reported in Fig. S3 and Table S2. Simulations of the tooth rasping at 8 different directions (see Fig. 5A) were performed using the commercially available finite element software (Abaqus) considering load control conditions. A maximum load of 1N was applied in each direction.

## 3. Results and discussion

### 3.1. The rasping behavior of Cryptochiton stelleri

Video analysis of the rasping behavior of *C. stelleri* revealed that during rasping, the chiton pulls the two rows of tricuspid teeth together like a zipper, as it pulls the entire radular membrane back into the buccal cavity (Fig. 2). During feeding, an odontophore pushes the anterior end of the radula against a rocky substrate, then retractor muscles contract, pulling the radula along the substrate containing algal deposits, raking food into its mouth (Nesson and Lowenstam, 1996) (Fig. 2A). A closer observation of the video suggests a differential loading on these teeth. The front of the tooth tip (leading edge) is loaded with the greatest mechanical load, but occasionally the tooth will snag on the substrate (i.e., rock or other surface) and rotate inwards towards the center of the radula (Fig. 2A). The motion of the tooth and stylus during rasping was schematically summarized using optical micrographs (Fig. 2B). Here, only mechanical loading from bending and twisting are taken into account.

The stylus is an essential part of the feeding system of chitons as it connects the ultrahard teeth with the flexible radular membrane and thereby enables the chiton to graze on rocky surfaces. Video analysis reveals the kinematics of the stylus during rasping and therefore helps to understand the direction of mechanical loading that is applied to the teeth. The rasping motion of *C. stelleri* is complex and involves four main steps. This leads to a complex distribution of positions in which different mechanical loads are applied to the teeth. This becomes more evident during feeding off of highly rough rocky substrates (Shaw et al., 2010), which yields a variation in tooth-rock contact and thus requires a flexible adaption. In order for the tooth to remove material from the substrate, adequate force must be applied through the stylus from the buccal musculature. Tensile forces must also be supported, as pulling, tearing, and ripping are part of *C. stelleri*'s feeding behavior, demonstrated by whole branches of algae found in the animal's intestinal tract (Meeuse and Flügel, 1958). Structures that are bent predictably in a single direction are most resistant to bending when the mass is distributed far from the bending axis (Wainwright et al., 1982). Hence, the macromorphological architecture of the stylus and the tooth likely play an important role for effective rasping.

### 3.2. Macromorphological architecture

Optical and SEM micrographs (Figs. 2B and 3, inset) reveal that the styli of *C. stelleri* possess a complex macromorphological architecture. The stylus is a highly contoured cylinder-like structure, which, together with the tooth, resembles a 'C'-shape. Each stylus is approximately 1 mm long and 0.4 mm in diameter. Arrows in the inset from Fig. 3 are used to

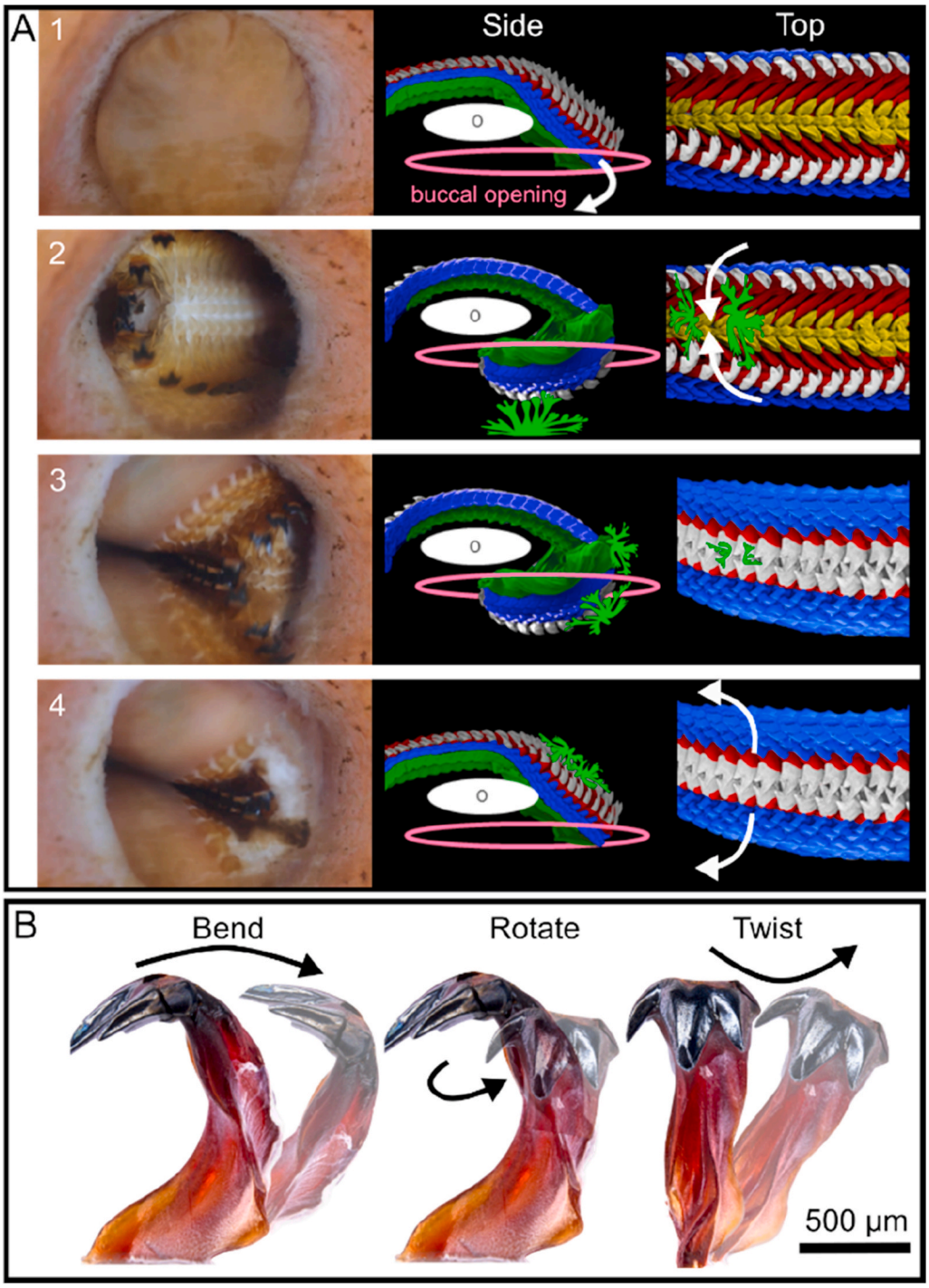


**Fig. 2.** Rasping behavior of C. stelleri. A1. The radular membrane is a flexible support A2. that bends around an odontophore during feeding (white arrow) on algal deposits (bright green structures). A3. Upon retraction through the buccal opening, the two rows of teeth are pulled together in a zipper-like manner, cutting through food and substrate alike. A4. Once retracted back into the mouth, the two rows of teeth can separate, releasing food and resetting the radula for the next rasping event. B. During retraction, the teeth are pulled together and scratching on the substrate causes a significant reorientation of the teeth. An overlay of optical micrographs shows that each tooth is loaded parallel to the long axis when the radula is pressed against the substrate, causing bending. Due to the 45° arrangement of major lateral teeth on the radular membrane, twisting occurs during retraction of the teeth into the mouth. The tooth is also able to rotate laterally as the flexible radula is bent around the odontophore during rasping. (For interpretation of the references to color in this figure legend, the reader is referred to the Web version of this article.)

highlight the directional motion referred in this study. The area of the stylus, which is connected with the radular belt is deemed the proximal end (bottom of the 'C'), whereas the top of the tooth is the distal end. The surface of the tooth that first makes contact with the substrate during rasping points towards the posterior end of the radular belt and is the leading edge of the tooth (inside of the 'C'). The opposite side towards the anterior end of the radular belt is the trailing edge of the tooth (backside of the 'C'). The side of the stylus and tooth that faces towards the center of the radular membrane is the medial side, while the side that faces the edge of the membrane is the lateral side.

µ-CT provides a detailed 3-dimensional macromorphological architecture of the stylus. The longitudinal section through the tooth and stylus as well as transverse cross-sections (perpendicular to the middle axis) at six different positions are shown in Fig. 3. The results show that the stylus has a non-circular, cross-section that varies as a function of its length. In addition, the µ-CT scan highlights that the stylus is not completely solid, but rather a tube-like structure. A hollow pore canal is found at the core of the stylus, running from the radular belt at the lower stylus zone and terminating below the junction zone.

The overall cross sections of each position (i.e., 1–6) are elongated. The centroid and second moment of area were calculated for each section to quantify the macroscopic morphology (Table 1). Based on these calculations, the stylus of the *C. stelleri* is found to twist along the length by 82°. This is observed by comparing the orientation of the cross-

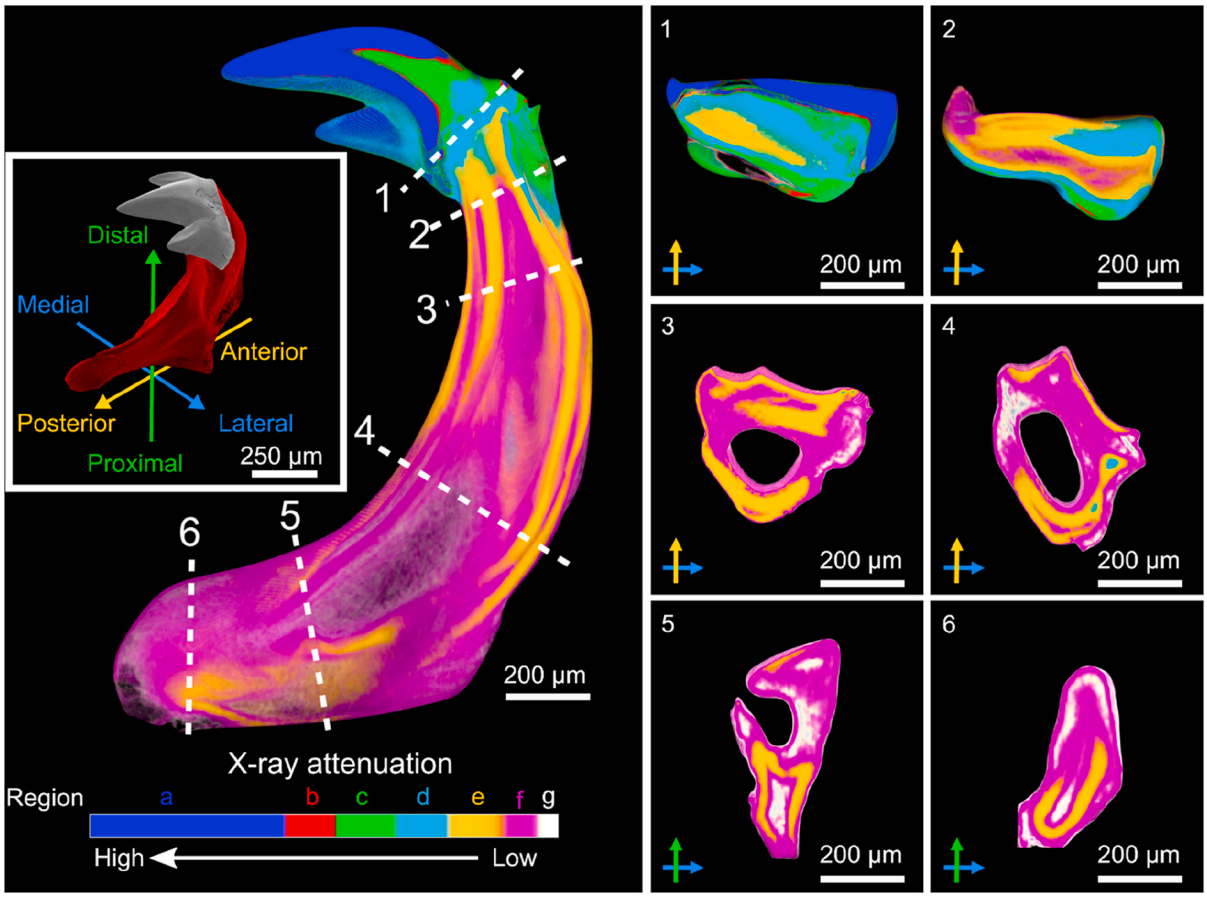


**Fig. 3.** µ-CT scans reveal that the stylus is a non-circular cylinder (containing a large pore canal) with a varied cross-sectional shape along its long axis. (Left image) Longitudinal section through the mid-plane of a µ-CT scan of the stylus and tooth. Color bar identifies areas (a–g) of relative X-ray attenuation in the structure (blue and white are the highest and lowest attenuations, respectively). The inset shows the false colored SEM micrograph (grey is the tooth and red is the stylus). Colored arrows denote the orientation of the cross-sections with respect to the distal and proximal ends, the posterior and anterior directions and the medial and lateral orientations. 1–6: Transverse cross-sections were taken from different heights along the length of the stylus, as indicated in the longitudinal section (left). (For interpretation of the references to color in this figure legend, the reader is referred to the Web version of this article.)

**Table 1**
The information obtained by nanoindentation and µ-CT on the transversal cross-sections were used to calculate the averaged reduced modulus ($E_r$) and the bending stiffness ($EI_x$, $EI_y$) along the long axis of the stylus.

| Cross-section | 1. | 2. | 3. | 4. | 5. | 6. |
|---|---|---|---|---|---|---|
| Averaged $E_r$ (GPa) | 18 | 16 | 15 | 14 | 12 | 12 |
| $E_{Ix}$ (Pa*m$^4$) | 2.64E-07 | 1.47E-07 | 3.15E-07 | 1.92E-07 | 6.66E-08 | 2.98E-08 |
| $E_{Iy}$(Pa*m$^4$) | 9.71E-07 | 9.44E-07 | 4.69E-07 | 4.44E-07 | 4.08E-07 | 1.71E-07 |

sections at positions 1 and 5 (Fig. 3). In addition, measurements (Fig. S2 and Table S1) show that the cross-sectional area of the stylus grows steadily from the proximal end (position 6) to the junction zone (position 1).

In order to provide mechanical support for the tooth, the macromorphology of the stylus is pivotal. The complex macromorphological architecture of the combined stylus-tooth structure resembles an arch, which distributes force throughout a larger volume of the structure, rather than concentrating the force at the tip (as observed in a straight morphology (van der Wal et al., 1999). Curvature in mammalian bone, for example, can change axial compression to bending, increasing its functionality in response to multiple load directions. While a straight column can support axial loads of much greater magnitude than a curved column, this design jeopardizes the structure when bending predominates (Bertram and Biewener, 1988). Hollow beams are known to be simultaneously flexible and robust against mechanical loading (Klein and Gänsicke, 2019). The highly contoured tubular shape of the stylus is optimized for this requirement as mass is only positioned where it is needed to fulfill the mechanical support function. Tubular structures consisting of materials with dissimilar properties are commonly found in Nature as they not only reduce weight, but also provide both stiffness and flexibility (Milwich et al., 2006; Zhao et al., 2010). For example, flying bird feathers are foam-filled cylinder-shaped lightweight materials tailored for withstanding mechanical load due to the aerodynamic drag during flying (Bachmann et al., 2012; Sullivan et al., 2016). In contrast, the pore canal in the stylus is open towards the proximal end of the stylus and is filled with body fluid and epithelial cells (Shaw et al., 2009). This not only reduces weight but may also minimize stress concentrations during rasping as the fluid can be released from the stylus into the surrounding epithelial tissue.

### 3.3. Nano-mechanical analysis

High-resolution nanoindentation mapping of polished longitudinal and transverse cross-sections (similar to those analyzed in µ-CT), reveal significant gradients in stiffness. Clearly, the longitudinal cross-section shows an increase in stiffness from the proximal end of the stylus, which is near the pore canal opening, to the distal region, which eventually is integrated through the junction zone, into the highly stiff tooth

(Fig. 4A). Interestingly, the stiffness of the "core" regions of the transverse cross sections is higher than those on the periphery in regions closer to the base of the stylus (i.e., proximal end), but is reversed (i.e., stiffer on the periphery) in regions 1 and 2 (approaching the junction zone). In fact, on the periphery of the junction zone, a region exists where the modulus values reach 23 GPa, which is close to the modulus of the chiton tooth core of 25 GPa (Weaver et al., 2010). This cross-section also shows cracking during sample preparation, which could be a sign for a remaining piece of tooth at the junction zone. The aforementioned observation is likely due to a combination of highly oriented, out of plane (from the transverse sections), and thus stiffer, alpha-chitin fibers located in the core of the stylus (Fig. S1) and mineral that is likely being introduced into the tooth from the stylus. In fact, neat the distal end of the stylus, the modulus is significantly higher in the leading or trailing edges. The highest modulus was measured in the junction zone and appears to blend into the leading and trailing edges. This heterogenous modulus distribution and the region-specific nature of stiffness in the stylus contribute to the balance of stiffness and flexibility of the stylus. The different regions within the stylus possess specific mechanical properties according to the mechanical load they are subjected to. Regions closer to the junction zone (near the tooth) have a higher stiffness in order to transduce force to the tooth, whereas regions closer to the proximal end are more flexible and thereby integrate the stylus with the flexible radula belt.

Based on the nanoindentation experiments as well as the μ-CT scan data, the averaged reduced modulus ($E_r$) and the bending stiffness' ($EI_x$, $EI_y$) of the stylus at each cross-section position were calculated (Table 1).

One main function of the stylus is to anchor the tooth to the radula belt and thereby generate a connection between these two dissimilar materials. The stylus as a whole resembles a functionally graded material. SEM micrographs of the stylus showed, in addition, that alpha-chitin fibers run through the junction zone towards the tooth (Fig. S1). Both, fibers and graded change in stiffness are enabling the strong attachment of the stylus to the tooth and the belt without generating sharp interfaces between the tooth and the stylus. Functional gradients combined with fiber-reinforced materials are a common principal in biological materials for the connection of dissimilar materials and reduce stress concentrations at the joint (Birman et al., 2013). The tooth attachment in the human periodontium, for example, includes two joints with graded stiffness: the connection between the alveolar bone and cementum and the interface between cementum and root dentin (Ho et al., 2007). These interfaces are also characterized by collagen fibers that run through the interface and form a fiber-reinforced material. Another example is the connection between tendon to bone (Thomopoulos et al., 2003). Here, the modulus changes in orders of magnitude within a small length scale and gradients in mineral content and fiber orientation were observed (Genin et al., 2009). A very steep gradient of mechanical properties was observed in the stylus, where the modulus changes from around 8 GPa–23 GPa within the length of the stylus. A gradation in modulus, like that observed along the length of the stylus, has been shown to increase failure resistance dramatically in structural materials (Suresh, 2001). Stiffness is added to this structure due to ridges that appear at the leading and the trailing edges. In many biological and engineered structures, ridges are implemented and lead to higher stiffness (Klein and Gänsicke, 2019; Purslow and Vincent, 1978). Some examples include ridges of cortical material, which run along two-thirds of the avian feather rachis (Bachmann et al., 2012) and the junction of the spike and bulb in the stomatopod dactyl club (Weaver et al., 2012). Ridged structures in cacti have been found to increase the surface to volume ratio so as not to apply stress to the epidermis during swelling, while also increasing the flexure stiffness of higher aspect ratio plants (Mauseth, 2000). This shows that the stylus has a complex multiscale morphology that is optimized not only for the attachment of the ultrahard tooth to the belt but also for mechanical support during rasping.

### 3.4. Regio-specific density distribution and elemental composition

In order to reveal the distribution of material in the stylus, X-ray attenuation data obtained by μ-CT were used (Davis et al., 2015, 2018; Gerward, 1993; Jackson and Hawkes, 1981). The color bar utilized in the μ-CT (Fig. 3) correlates with the X-ray attenuation normalized to the density of the material. The density of magnetite is known to be 5.15 g/cm$^3$ and represents the maximum attenuation (blue) while the density of air is 0.001225 g/cm$^3$ and represents the minimum attenuation (black). Furthermore, the density of pure chitin is 1.425 g/cm$^3$. Starting from these values, the densities of the different regions within the tooth-stylus structure were interpolated. A typical phantom like X-ray imaging reference is not applicable for this high-density material. Thus, we interpolated the X-ray attenuation from known densities of the magnetite (upper end) and chitin (low end), respectively. These maps reveal seven (Fig. 3, color bar a-g) spatially distinct regions of different density that run along the length of the stylus and into the tooth. These same regions coincide with those identified by nanoindentation and EDS.

The values for density obtained by X-ray attenuation in μ-CT scans and the moduli obtained by nanoindentation mapping show an overall gradient along the stylus long axis. The junction zone in the distal

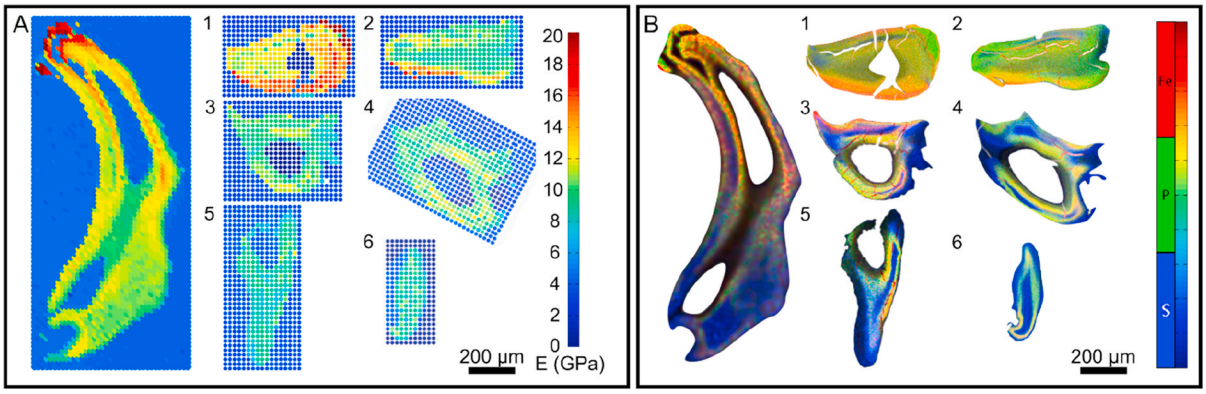


**Fig. 4.** Nanoindentation reveals strong correlation between mechanical properties and composition hinting at the function of various specific elements found in the stylus. A. Nanoindentation on a longitudinal section and six transversal cross-sections. This map shows a gradient along the length of the stylus, trending from 8 GPa in the lower stylus, to 23 GPa at the junction zone. Within transverse sections, the modulus can vary by 4 GPa within regions that are only 15 μm apart. Note: the maps are scaled to 20 GPa in order to enable comparison. Higher values are shown in darker red. B. EDS maps of the same longitudinal and transverse sections show that higher modulus values correlate with higher concentrations of iron and phosphorous. Lower modulus values correlate with a higher sulfur concentration and absence of iron and phosphorous. (For interpretation of the references to color in this figure legend, the reader is referred to the Web version of this article.)

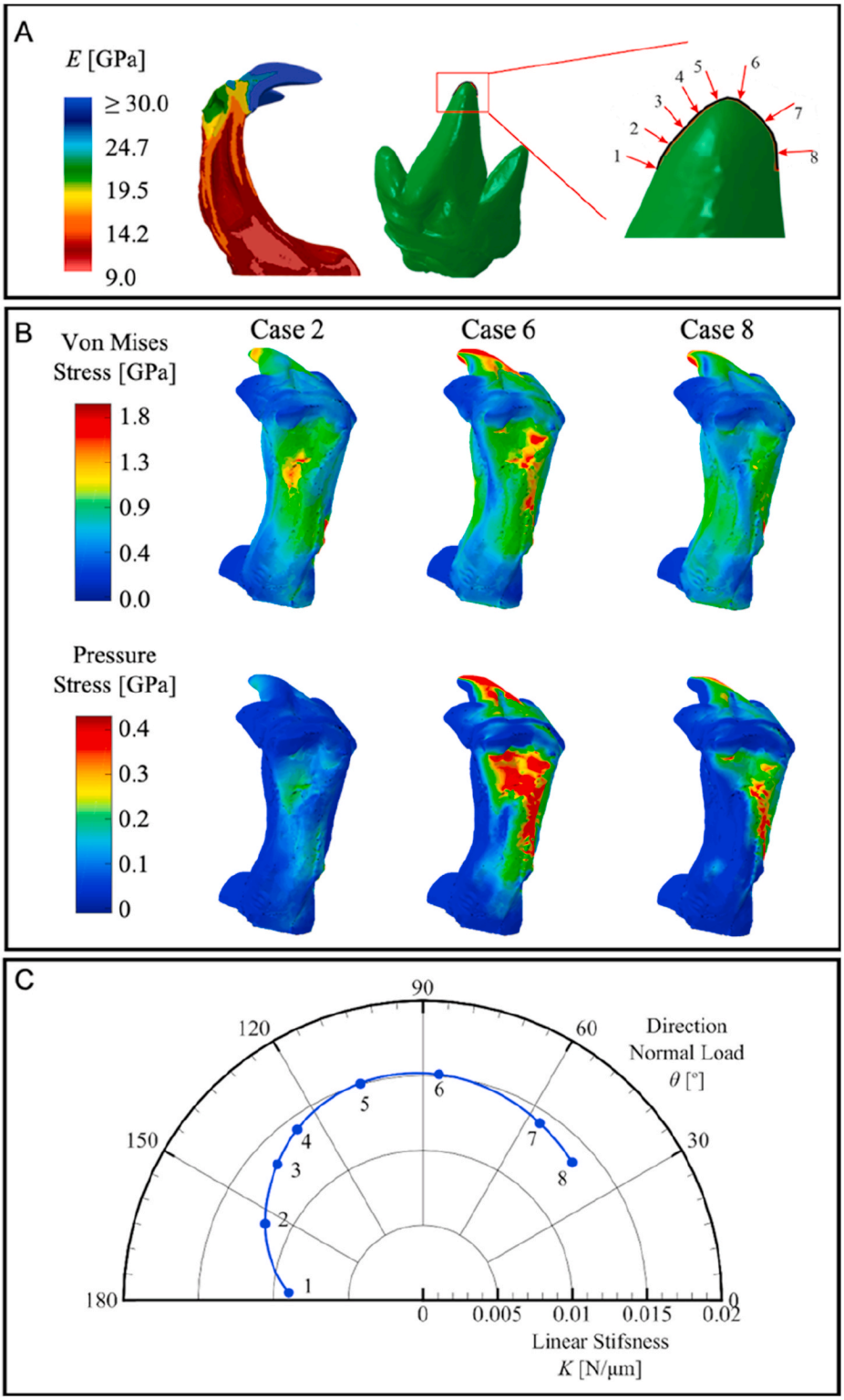


**Fig. 5.** The effect of loading direction on stresses of a non-circular tube. Simulation of tooth tip loading direction variation during rasping, and the stylus stress concentrations: A. The colormap shows the distribution of Youngs modulus in the tooth-stylus architecture. The diagram identifies loading directions for each case. Loading direction 1 applies force towards the medial direction. Loading direction 6 applies load to the tip of the tooth. Loading direction 8 applies force from the lateral direction. B. Von Mises and Pressure stress color maps for representative loading cases 2, 8 and 6. C. Linear stiffness as a function of the loading direction. (For interpretation of the references to color in this figure legend, the reader is referred to the Web version of this article.)

region, where the tooth is attached to the stylus is stiffer than the proximal region, where the stylus is attached to the flexible radula belt. In addition to this gradient, X-ray attenuation results show that there are distinct regions in which the mechanical properties are different due to different local material compositions. Furthermore, the bending stiffness' (Table 1) also show a similar trend, highlighting the fact that the stylus must be flexible enough to fold during retraction into the buccal cavity, while maintaining sufficient stiffness to transduce force to the tooth during rasping. The regions with higher densities are located closer to the junction zone and towards the trailing edge of the stylus, where a higher modulus is needed in order to enable mechanical support of the tooth. In contrast, the proximal regions of the stylus have a lower density and thereby are more flexible. Furthermore, the stylus is mainly composed of alpha-chitin fibers and proteins, with far less mineral than that in the tooth, and is thus less dense. In addition, the alpha-chitin fibers and proteins can provide stiffness. For example, chitin fibers

partially combined with minerals are found in the exoskeletons of many marine organisms (e.g., crab, shrimp and squid) as well as in insects. These composite materials are both stiff and lightweight (Gunderson and Schiavone, 1989; Vincent and Wegst, 2004).

However, EDS was used to determine if spatially distinct elemental distributions in the chiton stylus affected the stiffness of the material in specific regions. The same polished sections used for nanoindentation mapping were utilized for elemental analysis (Fig. 4B). In addition to C, O and N, varying quantities of Na, Cl, S, P, Ca, Mg, Fe, K, and Si were found (data not shown). Of these, we highlight iron, phosphorus and sulfur using false colored elemental X-ray maps: iron (red), phosphorus (green) and sulfur (blue). Longitudinal and transverse cross-sections reveal a strong correlation between the increase in reduced modulus and the presence of iron, phosphorous and sulfur. Although the stiffness is lower in the lower half of the stylus, the presence of sulfur likely provides a stiffening role via cross-linking of chitin fibers with proteins. Iron and phosphorus, which are found in the tooth as mineral components (Weaver et al., 2010), are also present in the distal end of the stylus and are likely either amorphous or inorganic precursor species. In fact, transmission electron microscopy (TEM) and selected area electron diffraction (SAED) analysis of the stylus at the distal end reveals that there may be amorphous/nanocrystalline mineral present (Fig. S1). This suggests that the stylus acts as a multifunctional structure that not only supports the tooth during rasping, but also enables iron and phosphorus transport, enabling biomineralization within the tooth.

### 3.5. Stress distribution in the stylus during rasping

The results obtained by μ-CT, X-ray attenuation and nanoindentation give insights to the macromorphological architecture and the local regiospecific mechanical properties of the stylus. These results reveal that the stylus is not a homogenous structure but has a higher modulus in the distal region and a lower modulus towards the proximal region. Within the tooth-stylus system, seven distinct regions with different material properties can be distinguished (Table S2 and Fig. S3). In order to understand the role of the varied regions within the stylus and to identify the stress distribution during the rasping process, finite element models (FEM) were used (Fig. 5). Eight different rasping conditions were simulated as shown in Fig. 5A, where the diagram identifies the loading directions for each case. Loading direction 1 applies force towards the medial direction. Loading direction 6 applies load to the tip of the tooth. Loading direction 8 applies force from the lateral direction. The von Mises and pressure stress distributions are reported for cases 2, 6 and 8 (Fig. 5B), while the linear stiffness was calculated as a function of loading direction (Fig. 5C). The loading directions were obtained by calculating the tangents to the tooth curvature in the 8 points shown in Fig. 5A.

In addition, the stress distributions (Fig. 6 and Fig. S3) are compared with each of the cross-sections presented in Fig. 4. The combination of the von Mises and pressure stress distributions provide information about the deviatoric and pressure components of the stress tensors for each loading condition. The von Mises and pressure stress maps in the structure show that the majority of stress is located in the shell of the tooth and the leading and trailing edges of the upper stylus (Fig. 5B). Also, it is possible to identify that the maximum stress distribution is generally located directly along the leading and trailing edge surfaces in the upper stylus. However, the stress is shifted towards the medial (or midline) side at the tooth elbow due to the overall geometry and the marginal lateral tooth support on the distal side. The FE simulations also show that larger stresses correlate with the same areas that have increased stiffness. Similar to other biological materials subjected to specific loading conditions, material distribution is not random but is likely organized to preserve the structural stability of the stylus during rasping (Fig. S4). It is important noting that the discontinuities in the stress profiles observed in Fig. 6 and Fig. S4 are due to the material mismatch between different regions. These material mismatches

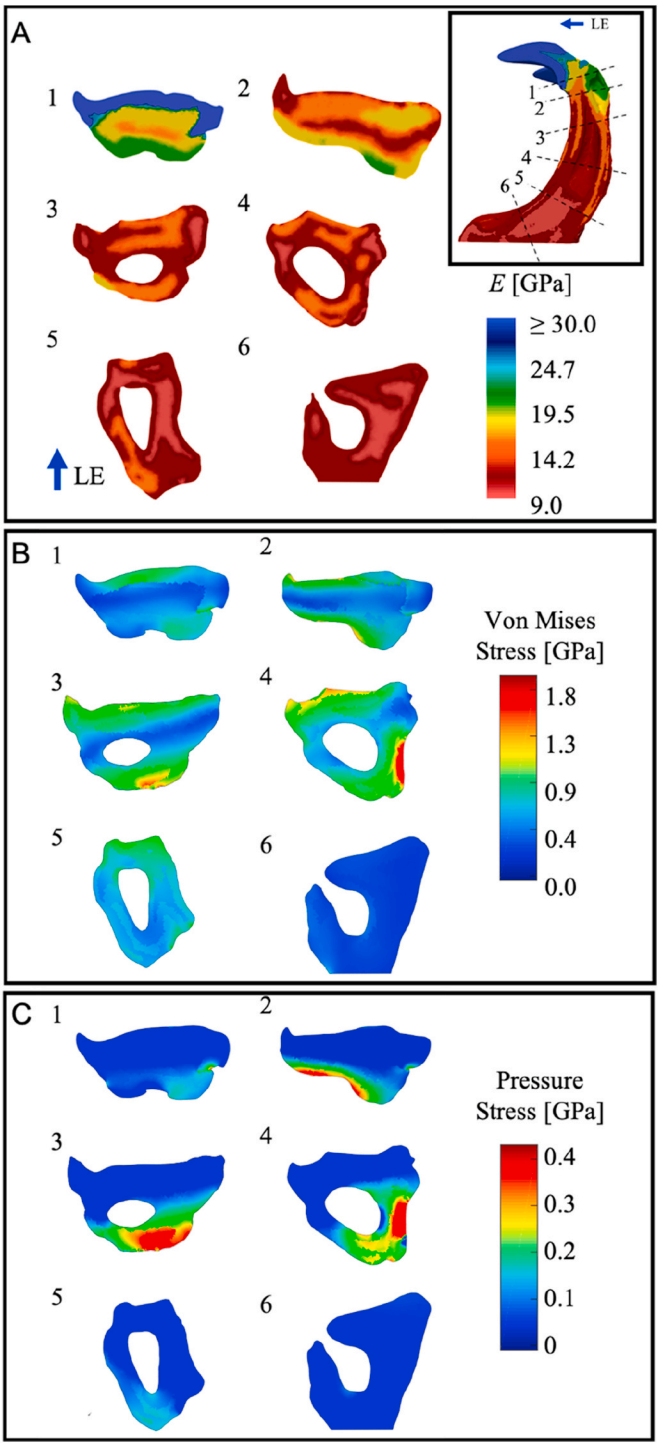


**Fig. 6.** Comparison of stress distribution when a force is applied in case 6 (case 2 and case 8 are shown in Fig. S4). A. Regio-specific distribution of the Elastic Modulus (E) along the stylus. B. Von Mises stress map. C. Pressure stress map.

correlate with our observations from X-ray attenuation and nanoindentation data. Different material distributions, including gradients at sets boundaries, are out of the scope of this study and are subject to future investigation.

The results also show that the combination between shape and material distribution favor the loading directly at the tip of the tooth, or along the proximal direction. As loading deviates away from the tip (cases 2 and 8), the linear stiffness of the stylus decreases, which enables the stylus to freely rotate and bend as shown in the videos (see video file

in supporting information, section S4). We hypothesize that this response allows for the safe release of the tooth during the rasping process, avoiding catastrophic damage. The finite element simulations show that the majority of stress is located in the same areas that have higher stiffness, primarily on the leading and trailing edges of the upper stylus. The stress is low towards the proximal end of the stylus because the marginal lateral tooth provides support and acts as a pivot point near the stylus elbow (Fig. S6).

Within the stylus, and the distribution of stiff material is regio-specific and co-localized with stress concentration. This complex structure combines flexible and stiff elements in order to enable force transduction and at the same time minimizes damage. The stylus has an exceptional role in the whole tooth-stylus-belt radula system as it connects the ultrahard teeth with the flexible radular belt. The interplay between these dissimilar parts enables the chitons to rasp on, and into, rough rocky surfaces in order to graze on algae. Hence, the stylus and the entire tooth-stylus-belt radula system of C. stelleri is a sophisticated structure from which inspiration can be drawn for many applications that need to be lightweight and flexible, yet provide mechanical strength and durability.

In many industrial produced devices, the connection of two or more parts composed of materials with very different properties is needed (Hu et al., 2011; Martinsen et al., 2015; Stokes, 1989). The durability and possibility to join dissimilar materials is especially interesting for the automotive (Araújo et al., 2017; Banea et al., 2017, 2018) and aerospace (Khan et al., 2018; Kumar et al., 2005; Quan et al., 2018; Scarselli et al., 2017) industries as integrating lightweight structures can lead to reduced emissions and fuel saving. Mechanical fastening, conventional welding or adhesive bonding are common techniques (Martinsen et al., 2015). Each technique offers advantages and disadvantages and can only be applied for specific material combinations and applications; however, joints are often prone to failure. In addition, most of the attachment methods add a third material to the material system (e.g., screw material, polymer adhesive) and thereby additional material properties and compatibilities need to be taken into account. One main role of the stylus is to anchor the ultrahard tooth to the flexible radula belt and, hence, the stylus provides inspiration for joining two different materials. The combination of fiber-reinforced and functionally graded material is a promising solution for the attachment of dissimilar materials.

Furthermore, the stylus itself, as well as the muscle actuated radula, provide potential models for soft robotic systems (Cianchetti et al., 2018; Gorissen et al., 2017; Gul et al., 2018; Kim et al., 2013; Shintake et al., 2018; Wallin et al., 2018). One main challenge of soft robotics is the control of deformability (Manti et al., 2016) and the integration of stiff and flexible elements in the same system. Here, the stylus, with its flexibility controlled by a combination macrostructural design elements with regio-specific distribution of stiff material can provide inspiration to a number of systems such as minimal invasive medical devices or actuators handling delicate objects. Furthermore, actuators moving in uncertain and uneven environments can be built inspired by the stylus rasping on rocky, rough surfaces. Clearly, structures inspired by the chitons' tooth-stylus-belt radula system provide potential to new biomimetic devices for applications in biomedicine, automotive and aerospace industry.

## 4. Conclusion and outlook

The stylus of *C. stelleri* is an example of a fiber-reinforced, functionally-graded structure that demonstrates effective integration of stiff and flexible components. With this combination of material properties, the stylus is able to maintain a firm connection between the soft radular belt and the ultrahard tooth cusp and transfers sufficient force from the radular musculature while minimizing the risk of catastrophic failure. The combination of high curvature and rotation of the major axis of its cross-section allows the stylus to delocalize stress during rasping events. Selectively denser regions in the upper stylus, enhanced by local fiber orientation parallel to its long axis and the presence of mineral components, provide both tensile and compressive strength to the leading edge and trailing edge, respectively. Utilizing the design principles provided by this multifunctional, flexible and lightweight natural composite may enable development of high-performance materials used in the medical, transportation, robotics, and defense industries.

## CRediT authorship contribution statement

**Anna Pohl:** Funding acquisition, Formal analysis, Visualization, Writing - review & editing. **Steven A. Herrera:** Funding acquisition, Formal analysis, Visualization, Writing - review & editing. **David Restrepo:** Methodology, Validation, Funding acquisition, Formal analysis, Visualization, Writing - review & editing. **Ryo Negishi:** Formal analysis. **Jae-Young Jung:** Funding acquisition, Formal analysis. **Chris Salinas:** Funding acquisition, Formal analysis. **Richard Wuhrer:** Funding acquisition, Formal analysis. **Tomoko Yoshino:** Writing - review & editing. **Joanna McKittrick:** Writing - review & editing. **Atsushi Arakaki:** Writing - review & editing. **Michiko Nemoto:** Writing - review & editing. **Pablo Zavattieri:** Conceptualization, Methodology, Formal analysis, Visualization, Writing - review & editing, Funding acquisition. **David Kisailus:** Conceptualization, Methodology, Formal analysis, Visualization, Writing - review & editing, Supervision, Project administration, Funding acquisition.

## Declaration of competing interest

The authors declare that they have no known competing financial interests or personal relationships that could have appeared to influence the work reported in this paper.

## Acknowledgements

We acknowledge funding from the Air Force Office of Scientific Research, Award # FA9550-12-1-0249 and Award # FA9550-19-1-0286, and the Army Research Office, Award #W911NF-19-1-0347 and Award #W911NF-16-1-0208. We thank the Central Facility for Advanced Microscopy and Microanalysis at UC Riverside for providing electron microscopy equipment. R.N., T.Y., A.A. and D.K. also would like to thank to the support from Institute of Global Innovation Research (GIR) at TUAT.

## Appendix A. Supplementary data

Supplementary data to this article can be found online at https://doi.org/10.1016/j.jmbbm.2020.103991.

## References

Araújo, H.A.M., Machado, J.J.M., Marques, E.A.S., da Silva, L.F.M., 2017. Dynamic behaviour of composite adhesive joints for the automotive industry. Compos. Struct. 171, 549–561. https://doi.org/10.1016/j.compstruct.2017.03.071.

Bachmann, T., Emmerlich, J., Baumgartner, W., Schneider, J.M., Wagner, H., 2012. Flexural stiffness of feather shafts: geometry rules over material properties. J. Exp. Biol. 215 (Pt 3), 405–415. https://doi.org/10.1242/jeb.059451.

Banea, M.D., da Silva, L.F.M., Carbas, R., Campilho, R.D.S.G., 2017. Effect of material on the mechanical behaviour of adhesive joints for the automotive industry. J. Adhes. Sci. Technol. 31 (6), 663–676. https://doi.org/10.1080/01694243.2016.1229842.

Banea, M.D., Rosioara, M., Carbas, R.J.C., da Silva, L.F.M., 2018. Multi-material adhesive joints for automotive industry. Compos. B Eng. 151, 71–77. https://doi.org/10.1016/j.compositesb.2018.06.009.

Bertram, J.E.A., Biewener, A.A., 1988. Bone curvature: sacrificing strength for load predictability? J. Theor. Biol. 131 (1), 75–92. https://doi.org/10.1016/S0022-5193(88)80122-X.

Birman, V., Genin, G.M., Thomopoulos, S. (Eds.), 2013. Structural Interfaces and Attachments in Biology. Springer, New York, NY, p. 388. XII.

Blanc, L., Delchambre, A., Lambert, P., 2017. Flexible medical devices: review of controllable stiffness solutions. Actuators 6 (3), 23. https://doi.org/10.3390/act6030023.

Brooker, L.R., Shaw, J.A., 2012. The chiton radula: a unique model for biomineralization studies. In: Seto, J. (Ed.), Advanced Topics in Biomineralization. INTECH Open Access Publisher.
Caprino, G., 1984. Residual strength prediction of impacted CFRP laminates. J. Compos. Mater. 18 (6), 508–518. https://doi.org/10.1177/002199838401800601.
Chung, D.D.L., 2010. Composite Materials: Science and Applications. Springer, London, p. 371.
Chung, H., Das, S., 2008. Functionally graded Nylon-11/silica nanocomposites produced by selective laser sintering. Mater. Sci. Eng. A 487 (1–2), 251–257. https://doi.org/10.1016/j.msea.2007.10.082.
Cianchetti, M., Laschi, C., Menciassi, A., Dario, P., 2018. Biomedical applications of soft robotics. Nat Rev Mater 3 (6), 143–153. https://doi.org/10.1038/s41578-018-0022-y.
Davis, G.R., Evershed, A.N.Z., Mills, D., 2015. Characterisation of materials: determining density using X-ray microtomography. Mater. Sci. Technol. 31 (2), 162–166. https://doi.org/10.1179/1743284714Y.0000000618.
Davis, G.R., Mills, D., Anderson, P., 2018. Real-time observations of tooth demineralization in 3 dimensions using X-ray microtomography. J. Dent. 69, 88–92. https://doi.org/10.1016/j.jdent.2017.11.010.
Genin, G.M., Kent, A., Birman, V., Wopenka, B., Pasteris, J.D., Marquez, P.J., Thomopoulos, S., 2009. Functional grading of mineral and collagen in the attachment of tendon to bone. Biophys. J. 97 (4), 976–985. https://doi.org/10.1016/j.bpj.2009.05.043.
Gerward, L., 1993. X-ray attenuation coefficients: current state of knowledge and availability. Radiat. Phys. Chem. 41 (4), 783–789. https://doi.org/10.1016/0969-806X(93)90326-P.
Gorb, S.N., 2008. Biological attachment devices: exploring nature's diversity for biomimetics. Philosophical Transactions. Series A, Mathematical, Physical, and Engineering Sciences 366 (1870), 1557–1574. https://doi.org/10.1098/rsta.2007.2172.
Gorissen, B., Reynaerts, D., Konishi, S., Yoshida, K., Kim, J.-W., Volder, M. de, 2017. Elastic inflatable Actuators for soft robotic applications. Advanced materials (Deerfield Beach, Fla 29 (43). https://doi.org/10.1002/adma.201604977.
Grunenfelder, L.K., Herrera, S., Kisailus, D., 2014a. Crustacean-derived biomimetic components and nanostructured composites. Small 10 (16), 3207–3232. https://doi.org/10.1002/smll.201400559.
Grunenfelder, L.K., Obaldia, E.E. de, Wang, Q., Li, D., Weden, B., Salinas, C., Wuhrer, R., Zavattieri, P., Kisailus, D., 2014b. Stress and damage mitigation from oriented nanostructures within the radular teeth of Cryptochiton stelleri. Adv. Funct. Mater. 24 (39), 6093–6104. https://doi.org/10.1002/adfm.201401091.
Gul, J.Z., Sajid, M., Rehman, M.M., Siddiqui, G.U., Shah, I., Kim, K.-H., Lee, J.-W., Choi, K.H., 2018. 3D printing for soft robotics - a review. Sci. Technol. Adv. Mater. 19 (1), 243–262. https://doi.org/10.1080/14686996.2018.1431862.
Gunderson, S., Schiavone, R., 1989. The insect exoskeleton: a natural structural composite. J. Occup. Med. 41 (11), 60–63. https://doi.org/10.1007/BF03220386.
Ho, S.P., Marshall, S.J., Ryder, M.I., Marshall, G.W., 2007. The tooth attachment mechanism defined by structure, chemical composition and mechanical properties of collagen fibers in the periodontium. Biomaterials 28 (35), 5238–5245. https://doi.org/10.1016/j.biomaterials.2007.08.031.
Hu, S.J., Ko, J., Weyand, L., ElMaraghy, H.A., Lien, T.K., Koren, Y., Bley, H., Chryssolouris, G., Nasr, N., Shpitalni, M., 2011. Assembly system design and operations for product variety. CIRP Annals 60 (2), 715–733. https://doi.org/10.1016/j.cirp.2011.05.004.
Huang, W., Restrepo, D., Jung, J.-Y., Su, F.Y., Liu, Z., Ritchie, R.O., McKittrick, J., Zavattieri, P., Kisailus, D., 2019. Multiscale toughening mechanisms in biological materials and bioinspired designs. Adv. Mater. 31 (43), 1901561. https://doi.org/10.1002/adma.201901561.
Jackson, D.F., Hawkes, D.J., 1981. X-ray attenuation coefficients of elements and mixtures. Phys. Rep. 70 (3), 169–233. https://doi.org/10.1016/0370-1573(81)90014-4.
Kar, K.K.(E., 2016. Composite Materials: Processing, Applications, Characterizations, vol. XVII. Springer Berlin Heidelberg, p. 686.
Khan, M.A., Aglietti, G.S., Crocombe, A.D., Viquerat, A.D., Hamar, C.O., 2018. Development of design allowables for the design of composite bonded double-lap joints in aerospace applications. Int. J. Adhesion Adhes. 82, 221–232. https://doi.org/10.1016/j.ijadhadh.2018.01.011.
Kim, S., Laschi, C., Trimmer, B., 2013. Soft robotics: a bioinspired evolution in robotics. Trends Biotechnol. 31 (5), 287–294. https://doi.org/10.1016/j.tibtech.2013.03.002.
Kirschvink, J.L., Lowenstam, H.A., 1979. Mineralization and magnetization of chiton teeth: paleomagnetic, sedimentologic, and biologic implications of organic magnetite. Earth Planet Sci. Lett. 44 (2), 193–204. https://doi.org/10.1016/0012-821X(79)90168-7.
Klein, B., Gänsicke, T., 2019. Leichtbau-Konstruktion. Springer Fachmedien, Wiesbaden, XIV, p. 532.
Krumova, M., Klingshirn, C., Haupert, F., Friedrich, K., 2001. Microhardness studies on functionally graded polymer composites. Compos. Sci. Technol. 61 (4), 557–563. https://doi.org/10.1016/S0266-3538(00)00228-1.
Kumar, S.B., Sivashanker, S., Bag, A., Sridhar, I., 2005. Failure of aerospace composite scarf-joints subjected to uniaxial compression. Mater. Sci. Eng. A 412 (1–2), 117–122. https://doi.org/10.1016/j.msea.2005.08.033.
Lowenstam, H.A., Weiner, S., 1989. On Biomineralization. Oxford University Press, p. 336.
Macey, D.J., Brooker, L.R., 1996. The junction zone: initial site of mineralization in radula teeth of the chiton Cryptoplax striata (Mollusca: polyplacophora). J. Morphol. 230 (1), 33–42. https://doi.org/10.1002/(SICI)1097-4687(199610)230:1<33:AID-JMOR3>3.0.CO;2-O.
Mallick, P.K., 2007. Fiber-reinforced Composites: Materials, Manufacturing, and Design, third ed. CRC Press, Hoboken, p. 640.
Manti, M., Cacucciolo, V., Cianchetti, M., 2016. Stiffening in soft robotics: a review of the state of the art. IEEE Robot. Autom. Mag. 23 (3), 93–106. https://doi.org/10.1109/MRA.2016.2582718.
Martinsen, K., Hu, S.J., Carlson, B.E., 2015. Joining of dissimilar materials. CIRP Annals 64 (2), 679–699. https://doi.org/10.1016/j.cirp.2015.05.006.
Mauseth, J.D., 2000. Theoretical aspects of surface-to-volume ratios and water-storage capacities of succulent shoots. Am. J. Bot. 87 (8), 1107–1115. https://doi.org/10.2307/2656647.
Meeuse, B., Flügel, W., 1958. Carbohydrases in the sugar-gland juice of Cryptochiton (Polyplacophora, mollusca). Nature 181 (4610), 699–700. https://doi.org/10.1038/181699a0.
Meyers, M.A., Chen, P.-Y., Lin, A.Y.-M., Seki, Y., 2008. Biological materials: structure and mechanical properties. Prog. Mater. Sci. 53 (1), 1–206. https://doi.org/10.1016/j.pmatsci.2007.05.002.
Meyers, M.A., McKittrick, J., Chen, P.-Y., 2013. Structural biological materials: critical mechanics-materials connections. Science (New York, N.Y.) 339 (6121), 773–779. https://doi.org/10.1126/science.1220854.
Milwich, M., Speck, T., Speck, O., Stegmaier, Thomas, Heinrich, Planck, 2006. Biomimetics and technical textiles: solving engineering problems with the help of nature's wisdom. Am. J. Bot. 93 (10), 1455–1465. https://doi.org/10.3732/ajb.93.10.1455.
Moffat, K.L., Sun, W.-H.S., Pena, P.E., Chahine, N.O., Doty, S.B., Ateshian, G.A., Hung, C. T., Lu, H.H., 2008. Characterization of the structure-function relationship at the ligament-to-bone interface. Proc. Natl. Acad. Sci. U.S.A. 105 (23), 7947–7952. https://doi.org/10.1073/pnas.0712150105.
Naleway, S.E., Porter, M.M., McKittrick, J., Meyers, M.A., 2015. Structural design elements in biological materials: application to bioinspiration. Adv. Mater. 27 (37), 5455–5476. https://doi.org/10.1002/adma.201502403.
Nemoto, M., Wang, Q., Li, D., Pan, S., Matsunaga, T., Kisailus, D., 2012. Proteomic analysis from the mineralized radular teeth of the giant Pacific chiton, Cryptochiton stelleri (Mollusca). Proteomics 12 (18), 2890–2894. https://doi.org/10.1002/pmic.201100473.
Nesson, M.H., Lowenstam, H.A., 1996. Biomineralization processes of the radula teeth of chitons. In: Kirschvink, J.L., Jones, D.S., MacFadden, B.J. (Eds.), Magnetite Biomineralization and Magnetoreception in Organisms. A New Biomagnetism. Springer, Boston, MA.
Pharr, G.M., Strader, J.H., Oliver, W.C., 2009. Critical issues in making small-depth mechanical property measurements by nanoindentation with continuous stiffness measurement. J. Mater. Res. 24 (3), 653–666. https://doi.org/10.1557/jmr.2009.0096.
Pompe, W., Worch, H., Epple, M., Friess, W., Gelinsky, M., Greil, P., Hempel, U., Scharnweber, D., Schulte, K., 2003. Functionally graded materials for biomedical applications. Mater. Sci. Eng. A 362 (1), 40–60. https://doi.org/10.1016/S0921-5093(03)00580-X.
Purslow, P., Vincent, J.F.V., 1978. Mechanical properties of primary feathers from the pigeon. J. Exp. Biol. 72 (1), 251–260.
Quan, D., Urdániz, J.L., Rouge, C., Ivanković, A., 2018. The enhancement of adhesively-bonded aerospace-grade composite joints using steel fibres. Compos. Struct. 198, 11–18. https://doi.org/10.1016/j.compstruct.2018.04.071.
Ricketts, E.F., Calvin, J., Hedgpeth, J.W., Phillips, D.W., 1985. Between Pacific Tides. Stanford University Press, p. 680.
Scarselli, G., Corcione, C., Nicassio, F., Maffezzoli, A., 2017. Adhesive joints with improved mechanical properties for aerospace applications. Int. J. Adhesion Adhes. 75, 174–180. https://doi.org/10.1016/j.ijadhadh.2017.03.012.
Shao, Z.S., 2005. Mechanical and thermal stresses of a functionally graded circular hollow cylinder with finite length. Int. J. Pres. Ves. Pip. 82 (3), 155–163. https://doi.org/10.1016/j.ijpvp.2004.09.007.
Shaw, J.A., Macey, D.J., Brooker, L.R., Clode, P.L., 2010. Tooth use and wear in three iron-biomineralizing mollusc species. Biol. Bull. 218 (2), 132–144. https://doi.org/10.1086/BBLv218n2p132.
Shaw, J.A., Macey, D.J., Brooker, L.R., Stockdale, E.J., Saunders, M., Clode, P.L., 2009. The chiton stylus canal: an element delivery pathway for tooth cusp biomineralization. J. Morphol. 270 (5), 588–600. https://doi.org/10.1002/jmor.10705.
Shintake, J., Cacucciolo, V., Floreano, D., Shea, H., 2018. Soft Robotic Grippers. Advanced Materials. Deerfield Beach, Fla., e1707035 https://doi.org/10.1002/adma.201707035
Stokes, V.K., 1989. Joining methods for plastics and plastic composites: an overview. Polym. Eng. Sci. 29 (19), 1310–1324. https://doi.org/10.1002/pen.760291903.
Sullivan, T.N., Pissarenko, A., Herrera, S.A., Kisailus, D., Lubarda, V.A., Meyers, M.A., 2016. A lightweight, biological structure with tailored stiffness: the feather vane. Acta Biomater. 41, 27–39. https://doi.org/10.1016/j.actbio.2016.05.022.
Suresh, S., 2001. Graded materials for resistance to contact deformation and damage. Science (New York, N.Y.) 292 (5526), 2447–2451. https://doi.org/10.1126/science.1059716.
Thomopoulos, S., Birman, V., Genin, G.M., 2013. The challenge of attaching dissimilar materials. In: Birman, V., Genin, G.M., Thomopoulos, S. (Eds.), Structural Interfaces and Attachments in Biology. Springer, New York, NY, pp. 3–17.
Thomopoulos, S., Williams, G.R., Gimbel, J.A., Favata, M., Soslowsky, L.J., 2003. Variation of biomechanical, structural, and compositional properties along the tendon to bone insertion site. J. Orthop. Res. 21 (3), 413–419. https://doi.org/10.1016/S0736-0266(03)00057-3.

Towe, K.M., Lowenstam, H.A., 1967. Ultrastructure and development of iron mineralization in the radular teeth of Cryptochiton stelleri (mollusca). J. Ultra. Res. 17 (1), 1–13. https://doi.org/10.1016/S0022-5320(67)80015-7.

Udupa, G., Rao, S.S., Gangadharan, K.V., 2014. Functionally graded composite materials: an overview. Procedia Materials Science 5, 1291–1299. https://doi.org/10.1016/j.mspro.2014.07.442.

van der Wal, Paul, Giesen, H.J., Videler, John J., 1999. Radular teeth as models for the improvement of industrial cutting devices. Mater. Sci. Eng. C 7 (2), 129–142. https://doi.org/10.1016/S0928-4931(99)00129-0.

Vincent, J.F.V., Wegst, U.G.K., 2004. Design and mechanical properties of insect cuticle. Arthropod Struct. Dev. 33 (3), 187–199. https://doi.org/10.1016/j.asd.2004.05.006.

Wainwright, S.A., Biggs, W.D., Gosline, J.M., Currey, J.D., 1982. Mechanical Design in Organisms. Princeton University Press, p. 423.

Wallin, T.J., Pikul, J., Shepherd, R.F., 2018. 3D printing of soft robotic systems. Nat Rev Mater 3 (6), 84–100. https://doi.org/10.1038/s41578-018-0002-2.

Wang, Q., Nemoto, M., Li, D., Weaver, J.C., Weden, B., Stegemeier, J., Bozhilov, K.N., Wood, L.R., Milliron, G.W., Kim, C.S., DiMasi, E., Kisailus, D., 2013. Phase transformations and structural developments in the radular teeth of Cryptochiton stelleri. Adv. Funct. Mater. 23 (23), 2908–2917. https://doi.org/10.1002/adfm.201202894.

Weaver, J.C., Milliron, G.W., Miserez, A., Evans-Lutterodt, K., Herrera, S., Gallana, I., Mershon, W.J., Swanson, B., Zavattieri, P., DiMasi, E., Kisailus, D., 2012. The stomatopod dactyl club: a formidable damage-tolerant biological hammer. Science (New York, N.Y.) 336 (6086), 1275–1280. https://doi.org/10.1126/science.1218764.

Weaver, J.C., Wang, Q., Miserez, A., Tantuccio, A., Stromberg, R., Bozhilov, K.N., Maxwell, P., Nay, R., Heier, S.T., DiMasi, E., Kisailus, D., 2010. Analysis of an ultra hard magnetic biomineral in chiton radular teeth. Mater. Today 13 (1), 42–52. https://doi.org/10.1016/S1369-7021(10)70016-X.

Yaraghi, N.A., Guarín-Zapata, N., Grunenfelder, L.K., Hintsala, E., Bhowmick, S., Hiller, J.M., Betts, M., Principe, E.L., Jung, J.-Y., Sheppard, L., Wuhrer, R., McKittrick, J., Zavattieri, P.D., Kisailus, D., 2016. A sinusoidally architected helicoidal biocomposite. Adv. Mater. 28 (32), 6835–6844. https://doi.org/10.1002/adma.201600786.

Zhao, L., Ma, J., Wang, T., Xing, D., 2010. Lightweight design of mechanical structures based on structural bionic methodology. JBE 7 (4), S224–S231. https://doi.org/10.1016/S1672-6529(09)60239-0.